Testing scalar-tensor theories and PPN parameters in Earth orbit

Andreas Schärer,[1,*] Raymond Angélil,[2] Ruxandra Bondarescu,[1] Philippe Jetzer,[1] and Andrew Lundgren[3]

[1] *Department of Physics, University of Zurich, Winterthurerstrasse 190, 8057 Zurich, Switzerland*
[2] *Institute for Computational Science, University of Zurich, Winterthurerstrasse 190, 8057 Zurich, Switzerland*
[3] *Max Planck Institute for Gravitational Physics (Albert Einstein Institute), Callinstr. 38, 30167 Hannover, Germany*

(Dated: October 30, 2014)

We compute the PPN parameters γ and β for general scalar-tensor theories in the Einstein frame, which we compare to the existing PPN formulation in the Jordan frame for alternative theories of gravity. This computation is important for scalar-tensor theories that are expressed in the Einstein frame, such as chameleon and symmetron theories, which can incorporate hiding mechanisms that predict environment-dependent PPN parameters. We introduce a general formalism for scalar-tensor theories and constrain it using the limit on γ given by the Cassini experiment. In particular we discuss massive Brans-Dicke scalar fields for extended sources. Next, using a recently proposed Earth satellite experiment, in which atomic clocks are used for spacecraft tracking, we compute the observable perturbations in the redshift induced by PPN parameters deviating from their general relativistic values. Our estimates suggest that $|\gamma - 1| \sim |\beta - 1| \sim 10^{-6}$ may be detectable by a satellite that carries a clock with fractional frequency uncertainty $\Delta f/f \sim 10^{-16}$ in an eccentric orbit around the Earth. Such space experiments are within reach of existing atomic clock technology. We discuss further the requirements necessary for such a mission to detect deviations from Einstein relativity.

I. INTRODUCTION

General relativity (GR) is the widely accepted theory to explain gravitation. Nonetheless, there are other theories of gravity which also satisfy the experimental constraints and remain candidates for the correct theory of gravity. These theories are being constrained by various high precision experiments. In particular, the recent development of ultra-precise frequency standards and atom interferometers provide new opportunities for testing different aspects of gravity. In this paper, we focus on scalar-tensor theories, which are a class of alternative theories of gravity that in addition to the metric tensor include a scalar field. We are interested both in developing the theoretical framework for testing these theories and in estimating potential constraints from upcoming satellite missions that carry clocks in space.

Scalar-tensor theories are widely used in particle physics, string theory and cosmology to model poorly understood phenomena for which we may have some observations such as in the case of dark matter and dark energy, but the new physics remains tantalisingly just out of reach. Effective scalar fields can arise from underlying, not-yet understood fundamental physics such as compactified extra dimensions [1] or string theory, which includes the dilaton scalar field [2]. Since the detection of the Higgs particle [3] we know that scalar (spin-0) particles exist in nature. The phase of inflation [4], a short period of rapid expansion in the very early universe, could have been caused by a scalar field. Quintessence models make use of scalar fields causing the late-time acceleration of the universe and therefore they could replace the cosmological constant and explain dark energy [5]. These scalar fields may couple to matter in ways that slightly violate general relativity and could be detected as our instrumentation becomes more precise.

The most accessible testbed for theories of gravity is the external environment of compact bodies such as binary pulsars or solar system objects. Here the gravitational field is weak, allowing the use of the parametrized post-Newtonian formalism (PPN). While there are infinitely many possible frames, typically, the Lagrangians of these theories are expressed either in the Jordan or the Einstein frame. In the Jordan frame, the scalar field multiplies the Ricci scalar and any present matter fields couple directly to the frame metric, while in the Einstein frame the Ricci scalar appears alone (as in traditional Einstein gravity) and the matter fields couple to a conformally related metric. We focus on the γ and β parameters predicted by scalar-tensor theories for which we have existent experimental constraints.

The simplest scalar-tensor theory is the original Brans-Dicke theory, where the massless scalar field and its constant coupling function (in the Jordan frame) lead to $\gamma = (\omega_0 + 1)/(\omega_0 + 2)$ and $\beta = 1$ [6]. For the case of a massive Brans-Dicke field, which contains a potential $U \sim m^2\varphi^2$ in addition to the constant coupling, these parameters were determined in [7]. The introduction of the mass term induces the γ-parameter to become distance dependent. The parameters for chameleon theories were derived in [8]. In special cases, PPN parameters have been calculated for more general theories such as scalar-tensor-vector theories where, as its name implies, an additional vector field enters the stage of gravitation [9]. For general scalar-tensor theories formulated in the Jordan frame, they were determined in Hohmann *et al.* [10].

* andreas.schaerer@physik.uzh.ch

We calculate the PPN parameters for a general scalar-tensor theory expressed in the Einstein frame. We show how this formalism can be useful for finding the PPN parameters for specific choices of scalar-tensor theories. Next, turning to a variety of scalar-tensor theories which predict constant PPN parameters, we investigate the near-future prospects for the measurement of deviations from Einstein relativity using a class of Earth-orbiting atomic clock experiments introduced in our earlier work, Angélil *et al.* [11].

The PPN parameters are typically calculated for a spacetime consisting of a point source surrounded by vacuum. This assumption is, in general, not appropriate to solve the scalar field equation of motion. For example in chameleon scalar field theories [12] or symmetron theories [13], the field behaves in a complex way inside the Earth due to its high density, significantly altering the external field profile. This also implies that the PPN parameters can depend on the environment. Performing an experiment around Earth may reveal different PPN parameters compared to the same experiment performed in the vicinity of the Sun.

Therefore, to discuss constraints on the PPN parameters in general we introduce a simple formalism containing a free parameter which can depend on the properties of both the theory and the source mass under consideration. It can account for the effects arising from the finite size of the source like screening effects in chameleon theories. We solve the scalar field equation for a massive Brans-Dicke scalar field in- and outside a sphere of constant density and show that our ansatz indeed represents the typical field profile of a massive scalar. The most stringent constraint in the solar system comes from measurements of the Cassini spacecraft, which limit the size of the γ PPN parameter around the Sun [14]. We use this limit to improve constraints on massive Brans-Dicke theory discussed in [7, 10] by regarding the Sun as a homogeneous sphere instead of a point source. However, while the Sun has low density, it is not an ideal candidate to probe theories that propose hiding mechanisms due to its high compactness M/R. The Earth and the Moon are more suitable due to their lower compactness to test theories such as chameleon theories.

In the second part of the paper, we bring attention to the increasing accuracy of space-qualified atomic clocks. Our estimates show that a space clock that can reach the accuracy of the Atomic Clock Ensemble in Space [15] $\Delta f/f \sim 10^{-16}$ in an eccentric orbit around the Earth could place constraints on the β and γ PPN parameters around the Earth of about 10^{-6} over the course of one orbit. It can be expected that in future, many space missions will use either an ultra-precise atomic clock or a transponder that can reflect signals from other clocks on Earth and in space to track the spacecraft. These will allow the ability to constrain or detect signals from alternative theories of gravity. The estimates presented here are obtained by taking the difference between the redshift signal generated by general relativity $\gamma = \beta = 1$, and the signal generated by a theory with γ and β different from one. The numbers obtained here are large enough to suggest detectability if a clock-carrying mission on an orbit like that of the originally proposed satellite Space-Time Explorer and QUantum Equivalence Principle Test (STE-QUEST) were to fly [16]. However, to make any definitive statements further work that aims to recover the signal of specific alternative theory of gravity from realistic data would be needed. We show that the difference in the redshift signal between general relativity and a small deviation peaks around pericenter. We study the width of these peaks to find the time scale which needs to be resolved in order to be sensitive to such deviations.

The outline of this paper is as follows. In section II A, the parametrized post-Newtonian formalism is briefly reviewed. Section II B discusses the action and the equations of motion of a scalar-tensor theory in both the Jordan and the Einstein frame. The conformal transformation relating these frames is addressed, whereas more details can be found in appendix A. After briefly reviewing the procedure to obtain the PPN parameters in the Jordan frame in II C, we calculate these parameters in detail for any theory formulated in the Einstein frame in section II D. In section III, we address constraints on scalar theories. We bring attention to the importance of screening mechanisms and propose a simple framework to constrain scalar theories and discuss current and future experimental constraints. Note that in this paper we restrict attention to local constraints on the PPN parameters and do not discuss cosmological constraints on chameleon models. We apply this formalism to some examples: (A) Brans-Dicke theory, the simplest case of a scalar-tensor theory, (B) massless fields with a more general coupling, (C) massive Brans-Dicke theory and (D) chameleon fields, an example for a field with a screening mechanism. Next, in section IV, we address the possibility of constraining PPN parameters in Earth orbit using satellites endowed with state-of-the-art atomic clocks. To do so, we estimate the relativistic effects coming from varying PPN parameters using a numerical orbit simulation.

Throughout this work we set the units to $c = \hbar = 1$, and therefore the reduced Planck mass is $M_{\rm Pl} = \sqrt{1/8\pi G}$.

II. SCALAR-TENSOR THEORIES IN THE EINSTEIN FRAME

A. The Parametrized Post-Newtonian Formalism

The most common way to parametrize theories of gravity in the weak field is to use the parametrized post-Newtonian (PPN) formalism [17]. There, the standard general relativistic metric is generalized with a collection of parameters which are permitted to take any value decreed by the alternative theory under consideration.

We start with the Schwarzschild metric written in

isotropic coordinates $(t, \chi, \theta, \varphi)$

$$\begin{aligned} ds^2 &= g_{\mu\nu} dx^\mu dx^\nu \\ &= -\frac{\left(1-\frac{GM}{2\chi}\right)^2}{\left(1+\frac{GM}{2\chi}\right)^2} dt^2 + \left(1+\frac{GM}{2\chi}\right)^4 (d\chi^2 + \chi^2 d\Omega^2), \end{aligned} \tag{1}$$

where $d\Omega := d\theta^2 + \sin^2\theta d\varphi^2$. This is the vacuum solution of the Einstein field equations outside a spherically symmetric non-charged and non-rotating mass M. G denotes the Newtonian gravitational constant. In this paper, we are interested in solar system constraints and since within the solar system gravitational fields are weak and typical velocities are small, it is sufficient to consider the post-Newtonian limit of this metric. To do so, we introduce a parameter ϵ. Its power tracks the order of a term, where $\epsilon \sim GM/r$, although numerically $\epsilon = 1$. Massive particles moving on an orbit typically have velocities $v^2 \approx GM/r$ and therefore $\epsilon \sim v^2$ (Note that other authors use the convention $\epsilon \sim v$). Typically, we have $GM/r \ll 1$ within the solar system. Therefore, after endowing the different terms in the Schwarzschild metric with the appropriate ϵ^n, we can perform an expansion in ϵ and neglect higher order terms. For the post-Newtonian level, we keep terms up to order ϵ^2 in g_{00} and up to order ϵ in g_{ij}. Many alternative theories of gravity predict solutions which start to deviate from the ones predicted by general relativity at this level. Therefore, the parameters γ and β are added to the metric to model deviations from general relativity ($\gamma = \beta = 1$) [17]. Here, we promote the γ and β from constants to functions of χ. Additionally, the gravitational 'constant' is allowed to change with distance.

This gives the metric

$$\begin{aligned} ds_{\mathrm{J}}^2 = &-\left(1 - h^{(1)}_{\mathrm{J}00}(\chi)\epsilon - h^{(2)}_{\mathrm{J}00}(\chi)\epsilon^2\right) dt_{\mathrm{J}}^2 \\ &+ \left(1 + h^{(1)}_{\mathrm{J}\chi\chi}(\chi)\epsilon\right)\left(d\chi^2 + \chi^2 d\Omega^2\right) \end{aligned} \tag{2}$$

with

$$\begin{aligned} h^{(1)}_{\mathrm{J}00}(\chi) &= \frac{2G_{\mathrm{J}}(\chi)M_{\mathrm{J}}}{\chi} \\ h^{(1)}_{\mathrm{J}\chi\chi}(\chi) &= \gamma(\chi)\frac{2G_{\mathrm{J}}(\chi)M_{\mathrm{J}}}{\chi} \\ h^{(2)}_{\mathrm{J}00}(\chi) &= -\beta(\chi)\frac{4G_{\mathrm{J}}^2(\chi)M_{\mathrm{J}}^2}{2\chi^2}. \end{aligned} \tag{3}$$

The index J indicates that this metric is formulated in the Jordan frame (see next section). Note that if more intricate spacetimes are considered, additional parameters may enter the metric.

B. The choice of frame

The action of a scalar-tensor theory can be written in various ways. In the Jordan frame it is

$$\begin{aligned} S = &\int d^4x\sqrt{-g_{\mathrm{J}}}\frac{M_{\mathrm{Pl}}^2}{2}\left[\varphi R_{\mathrm{J}} - \frac{\omega(\varphi)}{\varphi}\left(\nabla_{\mathrm{J}}\varphi\right)^2 - U(\varphi)\right] \\ &+ \int d^4x\sqrt{-g_{\mathrm{J}}}\mathcal{L}^{\mathrm{J}}_{\mathrm{m}}(\Phi_{\mathrm{m}}, g^{\mathrm{J}}_{\mu\nu}), \end{aligned} \tag{4}$$

where the theory is characterized by the coupling function $\omega(\varphi)$ and the scalar potential $U(\varphi)$, both functions of the scalar field. The scalar field is considered to be positive everywhere and we assume that $U \geq 0$ and $\omega > -3/2$.

There are two characteristic properties of this frame. First, the non-minimally coupling term φR_{J} represents the coupling between the scalar field and curvature. Second, matter fields Φ_{m} couple to the frame metric $g^{\mathrm{J}}_{\mu\nu}$ which is used to determine the Christoffel symbols, the Ricci tensor, and to raise and lower indices. By varying this action with respect to the metric and the scalar field, the tensor and the scalar equations of motion

$$\begin{aligned} R^{\mathrm{J}}_{\mu\nu} = &\frac{1}{\varphi}\left[8\pi G\left(T^{\mathrm{J}}_{\mu\nu} - \frac{\omega+1}{2\omega+3}g^{\mathrm{J}}_{\mu\nu}T_{\mathrm{J}}\right) + \nabla^{\mathrm{J}}_\mu\partial_\nu\varphi\right. \\ &+ \frac{\omega}{\varphi}\partial_\mu\varphi\partial_\nu\varphi \quad - \frac{1}{2}g^{\mathrm{J}}_{\mu\nu}\frac{1}{2\omega+3}\frac{\partial\omega}{\partial\varphi}(\nabla_{\mathrm{J}}\varphi)^2 \\ &\left.+ \frac{1}{2}g^{\mathrm{J}}_{\mu\nu}\frac{2\omega+1}{2\omega+3}U + \frac{1}{2}g^{\mathrm{J}}_{\mu\nu}\frac{1}{2\omega+3}\varphi\frac{\partial U}{\partial\varphi}\right] \end{aligned} \tag{5a}$$

$$\nabla^2_{\mathrm{J}}\varphi = \frac{1}{2\omega+3}\left(8\pi G T_{\mathrm{J}} - \omega_{,\varphi}\left(\nabla_{\mathrm{J}}\varphi\right)^2 - 2U + \varphi U_{,\varphi}\right) \tag{5b}$$

are obtained, where $\nabla^2_{\mathrm{J}} := g^{\mu\nu}_{\mathrm{J}}\nabla^{\mathrm{J}}_\mu\partial_\nu$. By ∇^{J}_μ we denote the covariant derivative obtained from the Jordan frame metric. By $T^{\mathrm{J}}_{\mu\nu}$ and $T_{\mathrm{J}} = g^{\mu\nu}_{\mathrm{J}}T^{\mathrm{J}}_{\mu\nu}$ we denote the stress-energy tensor and its trace in the Jordan frame.

Alternatively, a scalar-tensor theory can be expressed in the Einstein-frame

$$\begin{aligned} S = &\int d^4x\sqrt{-g_{\mathrm{E}}}\frac{M_{\mathrm{Pl}}^2}{2}\left[R_{\mathrm{E}} - 2(\nabla_{\mathrm{E}}\phi)^2 - V(\phi)\right] \\ &+ \int d^4x\sqrt{-g_{\mathrm{E}}}\mathcal{L}^{\mathrm{E}}_{\mathrm{m}}(\Phi_{\mathrm{m}}, F(\phi)^{-1}g^{\mathrm{E}}_{\mu\nu}) \end{aligned} \tag{6}$$

with the corresponding equations of motion

$$R^{\mathrm{E}}_{\mu\nu} = 8\pi G\left(T^{\mathrm{E}}_{\mu\nu} - \frac{1}{2}g^{\mathrm{E}}_{\mu\nu}T_{\mathrm{E}}\right) + 2\partial_\mu\phi\partial_\nu\phi + \frac{1}{2}g^{\mathrm{E}}_{\mu\nu}V(\phi) \tag{7a}$$

$$\nabla^2_{\mathrm{E}}\phi = \frac{8\pi G}{4}\frac{F_{,\phi}}{F}T_{\mathrm{E}} + \frac{1}{4}V_{,\phi}. \tag{7b}$$

Here, the theory is determined by the coupling function $F(\phi)$ and the potential $V(\phi)$. In this frame, the field couples minimally to gravity and therefore, the gravity

part of the action takes the form of the Einstein-Hilbert action in general relativity. This comes at the price that the matter fields do not couple to the Einstein frame metric directly but to the combination $F(\phi)^{-1}g^{\rm E}_{\mu\nu}$, and therefore, the coupling explicitly depends on the scalar field. But there is an obvious advantage when working in the Einstein frame: there, the equations of motion (7) are much simpler compared to the ones in the Jordan frame (5), even though these two frames are mathematically equivalent.

To avoid confusion between these two frames we label quantities with indices J and E, depending on the frame they are coming from. The two frames are related to each other by a conformal transformation

$$g^{\rm J}_{\mu\nu} = F(\phi)^{-1} g^{\rm E}_{\mu\nu} \tag{8}$$

with $\varphi = F > 0$, i.e. the scalar field in the Jordan frame mimics the coupling function in the Einstein frame. The positiveness of the fields is required to avoid a change of sign in the metric line element when going from one to the other frame. This conformal transformation is discussed in appendix A.

C. PPN parameters in the Jordan frame

The PPN parameters γ and β have been calculated for a general scalar-tensor theory stated in the Jordan frame [10]. Here we give a very short overview of their derivation. One starts with the ansatz for the metric (2) where χ is the radial coordinate in isotropic coordinates. Expanding the scalar field φ, the coupling function ω and the potential U in powers of ϵ (see appendix A) and solving the equations of motion (5) order by order, one finds [10]

$$G_{\rm J}(\chi) = \frac{G}{\varphi_0}\left(1 + \frac{1}{2\omega_0+3}e^{-m_{\rm J}\chi}\right) \tag{9a}$$

$$\gamma(\chi) = \frac{1 - \frac{1}{2\omega_0+3}e^{-m_{\rm J}\chi}}{1 + \frac{1}{2\omega_0+3}e^{-m_{\rm J}\chi}} \tag{9b}$$

$$\begin{aligned}\beta(\chi) = 1 &+ \frac{\varphi_0\omega_1}{(2\omega_0+3)^3\left(1+\frac{e^{-m_{\rm J}\chi}}{2\omega_0+3}\right)^2}e^{-2m_{\rm J}\chi} \\ &+ \frac{m_{\rm J}\chi}{2(2\omega_0+3)\left(1+\frac{e^{-m_{\rm J}\chi}}{2\omega_0+3}\right)^2}\Big[2e^{-m_{\rm J}\chi}\ln(m_{\rm J}\chi) - e^{-2m_{\rm J}\chi} - 2\left(m_{\rm J}\chi + e^{m_{\rm J}\chi}\right)\mathrm{Ei}(-2m_{\rm J}\chi) \\ &+ \frac{3\varphi_0}{2\omega_0+3}\left(\frac{U_3}{U_2} - \frac{1}{\varphi_0} - \frac{\omega_1}{2\omega_0+3}\right)\left[e^{-m_{\rm J}\chi}\mathrm{Ei}(-m_{\rm J}\chi) - e^{m_{\rm J}\chi}\mathrm{Ei}(-3m_{\rm J}\chi)\right]\Big],\end{aligned} \tag{9c}$$

where

$$m_{\rm J} := \sqrt{\frac{2U_2\varphi_0}{2\omega_0+3}} \tag{10}$$

can be interpreted as the inverse range of the field or, roughly speaking, the mass of the field. In this expression we use the notation $U_2 = U''(\varphi_0)/2$. Here we make use of the exponential integral

$$\mathrm{Ei(-x)} := -\int_x^\infty da\frac{e^{-a}}{a}. \tag{11}$$

D. PPN parameters in the Einstein frame

In this section, we complement the Hohmann *et al.* [10] approach by calculating the PPN parameters for a general scalar-tensor theory formulated in the Einstein-frame. To do so, the equations of motion are solved order-by-order in the Einstein frame. Finally, we transform to the Jordan frame where the PPN parameters are defined. For the sake of understandability we perform the calculation in detail.

Here we consider a spacetime consisting of a point mass surrounded by vacuum. The stress-energy tensor is given by that of a perfect fluid [17]

$$T^{\mu\nu} = (\rho + \rho\Pi + p)\,u^\mu u^\nu + p g^{\mu\nu}, \tag{12}$$

with the rest-mass density ρ, the pressure p, the specific energy density Π and the four-velocity u^μ, satisfying $u_\mu u^\mu = -1$. For solar system tests we typically have $\rho \gg p$ and $\rho \gg \rho\Pi$, so we may neglect both the effects of pressure and specific energy density. If the mass is at rest ($u^i = 0$), we obtain $T_{\mu\nu} = \mathrm{diag}(\rho, 0, 0, 0)$. For a point source we have $\rho_{\rm E} = M_{\rm E}\delta(r)\epsilon$, where the index E implies that a quantity is defined in the Einstein frame.

For the metric in the Einstein frame we make the

ansatz

$$\begin{aligned} ds_{\rm E}^2 = &-\left(1-h^{(1)}_{\rm E00}(r)\epsilon - h^{(2)}_{\rm E00}(r)\epsilon^2\right)dt_{\rm E}^2\epsilon^2 \\ &+\left(1+h^{(1)}_{{\rm E}rr}(r)\epsilon\right)\left(dr^2+r^2d\Omega^2\right), \end{aligned} \tag{13}$$

where we choose isotropic coordinates with radial coordinate r. We expand the scalar field in powers of ϵ and subsequently the coupling function and the potential are expanded around some constant value ϕ_0:

$$\phi(r) = \phi_0 + \phi_1(r)\epsilon + \phi_2(r)\epsilon^2 \tag{14a}$$

$$F(\phi) = F_0 + F_1\left(\phi-\phi_0\right) + F_2\left(\phi-\phi_0\right)^2 + F_3\left(\phi-\phi_0\right)^3 \tag{14b}$$

$$V(\phi) = V_0 + V_1\left(\phi-\phi_0\right) + V_2\left(\phi-\phi_0\right)^2 + V_3\left(\phi-\phi_0\right)^3 \tag{14c}$$

The left-hand sides of the equations (7a), the components of the Ricci tensor, are

$$\begin{aligned} R^{\rm E}_{00} = &-\frac{1}{2}\nabla_r^2 h_{\rm E00}\epsilon - \frac{1}{2}\Big(\nabla_r^2 h^{(2)}_{\rm E00} - h^{(1)}_{{\rm E}rr}\nabla_r^2 h^{(1)}_{\rm E00} \\ &+\frac{1}{2}(\partial_r h^{(1)}_{\rm E00})^2 + \frac{1}{2}(\partial_r h^{(1)}_{\rm E00})(\partial_r h^{(1)}_{{\rm E}rr})\Big)\epsilon^2 + \mathcal{O}(\epsilon^3) \end{aligned} \tag{15a}$$

$$R^{\rm E}_{rr} = \left(-\partial_r^2 h^{(1)}_{{\rm E}rr} - \frac{1}{r}\partial_r h^{(1)}_{{\rm E}rr} + \frac{1}{2}\partial_r^2 h^{(1)}_{\rm E00}\right)\epsilon + \mathcal{O}(\epsilon^2) \tag{15b}$$

$$R^{\rm E}_{\theta\theta} = \frac{1}{2}r^2\left(-\partial_r^2 h^{(1)}_{{\rm E}rr} - \frac{3}{r}\partial_r h^{(1)}_{{\rm E}rr} + \frac{1}{r}\partial_r h^{(1)}_{\rm E00}\right)\epsilon + \mathcal{O}(\epsilon^2) \tag{15c}$$

$$R^{\rm E}_{\varphi\varphi} = R^{\rm E}_{\theta\theta}\sin^2\theta + \mathcal{O}(\epsilon^2) \tag{15d}$$

to the required orders. All other components are identically zero. The right-hand sides are

$$\begin{aligned} R^{\rm E}_{\mu\nu} = &\frac{1}{2}\eta_{\mu\nu}V_0 + \Big[8\pi G\left(\delta^0_\mu\delta^0_\nu + \frac{1}{2}\eta_{\mu\nu}\right)M_{\rm E}\delta(r) \\ &+\frac{1}{2}\left(h^{(1)}_{{\rm E}\mu\nu}V_0 + \eta_{\mu\nu}V_1\phi_1\right)\Big]\epsilon \\ &+\Big[\frac{8\pi G}{2}\left(h^{(1)}_{{\rm E}\mu\nu} + \eta_{\mu\nu}h^{(1)}_{\rm E00}\right)M_{\rm E}\delta(r) \\ &+2\partial_r\phi_1\partial_r\phi_1\delta^r_\mu\delta^r_\nu + \frac{1}{2}\eta_{\mu\nu}V_2\phi_1^2 \\ &+\frac{1}{2}(h^{(1)}_{{\rm E}\mu\nu}\phi_1 + \eta_{\mu\nu}\phi_2)V_1\Big]\epsilon^2 + \mathcal{O}(\epsilon^3). \end{aligned} \tag{16}$$

The flat-space Minkowski metric is, with our choice of coordinates, $\eta_{\mu\nu} = \mathrm{diag}(-1, 1, r^2, r^2\sin^2\theta)$. Calculating both sides of the scalar equation yields

$$\begin{aligned} \nabla^2_{\rm E}\phi = &\nabla_r^2\phi_1\epsilon + \Big[\nabla_r^2\phi_2 - h^{(1)}_{{\rm E}rr}\nabla_r^2\phi_1 \\ &+\frac{1}{2}\left(\partial_r h^{(1)}_{{\rm E}rr} - \partial_r h^{(1)}_{\rm E00}\right)\partial_r\phi_1\Big]\epsilon^2 \end{aligned} \tag{17}$$

and

$$\begin{aligned} \nabla^2_{\rm E}\phi = &\frac{1}{4}V_1 + \left[-\frac{F_1}{F_0}2\pi G M_{\rm E}\delta(r) + \frac{1}{2}V_2\phi_1\right]\epsilon \\ &+\Big[\Big(2\pi G M_{\rm E}\left(\frac{F_1^2}{F_0^2} - \frac{2F_2}{F_0}\right)\phi_1 \\ &-2\pi G M_{\rm E}\frac{F_1}{F_0}h^{(1)}_{\rm E00}\Big)\delta(r) + \frac{3}{4}V_3\phi_1^2 + \frac{1}{2}V_2\phi_2\Big]\epsilon^2. \end{aligned} \tag{18}$$

By ∇_r^2 we mean the flat space spherical coordinate Laplace operator, $\nabla_r^2 := \partial_r^2 + 2/r\partial_r$. First, we consider the zeroth-order equations

$$0 = \frac{1}{2}\eta_{\mu\nu}V_0 \tag{19a}$$

$$0 = \frac{1}{4}V_1, \tag{19b}$$

which require $V_0 = V_1 = 0$. At first order in ϵ, the scalar equation is

$$\left(\nabla_r^2 - m_{\rm E}^2\right)\phi_1 = -\frac{F_1}{F_0}2\pi G M_{\rm E}\delta(r), \tag{20}$$

with solution

$$\phi_1(r) = \frac{F_1}{2F_0}\frac{GM_{\rm E}}{r}e^{-m_{\rm E}r}, \tag{21}$$

where we have defined

$$m_{\rm E}^2 := \frac{1}{2}V_2. \tag{22}$$

The first order 00-tensor equation and its solution are

$$\begin{aligned} -\frac{1}{2}\nabla_r^2 h_{\rm E00} &= 8\pi G\frac{1}{2}M_{\rm E}\delta(r) \\ \rightarrow \quad h_{\rm E00}(r) &= \frac{2GM_{\rm E}}{r}. \end{aligned} \tag{23}$$

At the same order, the rr-equation is

$$-\partial_r^2 h^{(1)}_{{\rm E}rr} - \frac{1}{r}\partial_r h^{(1)}_{{\rm E}rr} + \frac{1}{2}\partial_r^2 h^{(1)}_{\rm E00} = 8\pi G\frac{1}{2}M_{\rm E}\delta(r) \tag{24}$$

and the $\theta\theta$-equation turns into

$$-\partial_r^2 h^{(1)}_{{\rm E}rr} - \frac{3}{r}\partial_r h^{(1)}_{{\rm E}rr} + \frac{1}{r}\partial_r h^{(1)}_{\rm E00} = 8\pi G M_{\rm E}\delta(r). \tag{25}$$

Summing these two equations yields

$$\nabla_r^2 h^{(1)}_{{\rm E}rr} = -8\pi G M_{\rm E}\delta(r), \tag{26}$$

with solution

$$h^{(1)}_{{\rm E}rr}(r) = \frac{2GM_{\rm E}}{r}. \tag{27}$$

The 00-tensor equation at second order turns into

$$\nabla_r^2 h^{(2)}_{\rm E00} = -\frac{4G^2M_{\rm E}^2}{r^4} + \frac{F_1^2}{4F_0^2}V_2\frac{G^2M_{\rm E}^2}{r^2}e^{-2m_{\rm E}r^2}, \tag{28}$$

where we dropped a term proportional to $\delta(r)h^{(1)}_{\mathrm{E}rr}$ since it corresponds to gravitational self-energy [10] and we get the solution

$$h^{(2)}_{\mathrm{E}00}(r) = -\frac{4G^2M_\mathrm{E}^2}{2r^2}\Bigg[1 - \frac{F_1^2}{4F_0^2}\Bigg(\frac{1}{2}m_\mathrm{E}re^{-2m_\mathrm{E}r} + m_\mathrm{E}^2r^2\mathrm{Ei}(-2m_\mathrm{E}r)\Bigg)\Bigg]. \tag{29}$$

We notice that the metric component at post-Newtonian order has an additional term compared to the Schwarzschild metric of general relativity. The second order scalar field equation is

$$\nabla_r^2\phi_2 - h^{(1)}_{\mathrm{E}rr}\nabla_r^2\phi_1 + \frac{1}{2}\left(\partial_r h^{(1)}_{\mathrm{E}rr} - \partial_r h^{(1)}_{\mathrm{E}00}\right)\partial_r\phi_1 = \frac{3}{4}V_3\phi_1^2 + \frac{1}{2}V_2\phi_2. \tag{30}$$

Also here, we dropped the gravitational self-energy terms proportional to $\phi_1\delta(r)$, $h^{(1)}_{\mathrm{E}00}\delta(r)$ and $h^{(1)}_{\mathrm{E}rr}\delta(r)$. As solution we find

$$\begin{aligned}\phi_2(r) = {}& \frac{1}{4}\frac{F_1}{2F_0}m_\mathrm{E}\frac{4G^2M_\mathrm{E}^2}{r} \\ & \times\left[e^{m_\mathrm{E}r}\mathrm{Ei}(-2m_\mathrm{E}r) - e^{-m_\mathrm{E}r}\ln(m_\mathrm{E}r)\right] \\ & + \frac{1}{2m_\mathrm{E}}\frac{3F_1^2}{64F_0^2}V_3\frac{4G^2M_\mathrm{E}^2}{r} \\ & \times\left[e^{m_\mathrm{E}r}\mathrm{Ei}(-3m_\mathrm{E}r) - e^{-m_\mathrm{E}r}\mathrm{Ei}(-m_\mathrm{E}r)\right].\end{aligned} \tag{31}$$

We have thus solved the equations of motion to post-Newtonian order. To determine the PPN parameters we must turn to the Jordan frame where they are defined. The metric line elements in the two frames are related by the conformal transformation (8), giving

$$\begin{aligned}ds_\mathrm{J}^2 = {}& F(\phi)^{-1}ds_\mathrm{E}^2 \\ = {}& -\Bigg[1 - \left(h^{(1)}_{\mathrm{E}00} + \frac{F_1}{F_0}\phi_1\right)\epsilon - \Bigg(h^{(2)}_{\mathrm{E}00} - \frac{F_1}{F_0}h^{(1)}_{\mathrm{E}00}\phi_1 \\ & + \left(\frac{F_2}{F_0} - \frac{F_1^2}{F_0^2}\right)\phi_1^2 + \frac{F_1}{F_0}\phi_2\Bigg)\epsilon^2\Bigg]\frac{dt_\mathrm{E}^2}{F_0}, \\ & + \left[1 + \left(h^{(1)}_{\mathrm{E}rr} - \frac{F_1}{F_0}\phi_1\right)\epsilon\right]\left(\frac{dr^2}{F_0} + \frac{r^2}{F_0}d\Omega^2\right).\end{aligned} \tag{32}$$

Comparing this to the metric in the Jordan frame (2), we find

$$h^{(1)}_{\mathrm{J}00} = \frac{2G_\mathrm{J}M_\mathrm{J}}{\chi} \overset{!}{=} h^{(1)}_{\mathrm{E}00} + \frac{F_1}{F_0}\phi_1 \tag{33a}$$

$$h^{(1)}_{\mathrm{J}\chi\chi} = \gamma(\chi)\frac{2G_\mathrm{J}M_\mathrm{J}}{\chi} \overset{!}{=} h^{(1)}_{\mathrm{E}rr} - \frac{F_1}{F_0}\phi_1 \tag{33b}$$

$$\begin{aligned}h^{(2)}_{\mathrm{J}00} = {}& -\beta(\chi)\frac{4G_\mathrm{J}^2M_\mathrm{J}^2}{2\chi^2} \\ \overset{!}{=} {}& h^{(2)}_{\mathrm{E}00} - \frac{F_1}{F_0}h^{(1)}_{\mathrm{E}00}\phi_1 + \left(\frac{F_2}{F_0} - \frac{F_1^2}{F_0^2}\right)\phi_1^2 + \frac{F_1}{F_0}\phi_2\end{aligned} \tag{33c}$$

with

$$t_\mathrm{J} = \frac{t_\mathrm{E}}{\sqrt{F_0}} \tag{34a}$$

$$\chi = \frac{r}{\sqrt{F_0}}. \tag{34b}$$

From the $h^{(1)}_{\mathrm{J}00}$ relation we can identify the effective gravitational 'constant' in the Jordan frame

$$G_\mathrm{J}(r) = \frac{r}{2F_0M_\mathrm{E}}\left(h^{(1)}_{\mathrm{E}00} + \frac{F_1}{F_0}\phi_1\right), \tag{35}$$

where the masses in the Jordan frame satisfy

$$m_\mathrm{J} = \sqrt{F_0}m_\mathrm{E} \tag{36a}$$

$$M_\mathrm{J} = \sqrt{F_0}M_\mathrm{E}, \tag{36b}$$

such that $m_\mathrm{J}\chi = m_\mathrm{E}r$. With this we obtain the γ parameter

$$\gamma(r) = \frac{h^{(1)}_{\mathrm{E}rr} - \frac{F_1}{F_0}\phi_1}{h^{(1)}_{\mathrm{E}00} + \frac{F_1}{F_0}\phi_1}. \tag{37}$$

And finally, the β parameter is

$$\begin{aligned}\beta(r) &= \frac{2\chi^2}{4G_\mathrm{J}^2(r)M_\mathrm{J}^2}\left[\frac{F_1}{F_0}h^{(1)}_{\mathrm{E}00}\phi_1 - \left(\frac{F_2}{F_0} - \frac{F_1^2}{F_0^2}\right)\phi_1^2 - \frac{F_1}{F_0}\phi_2 - h^{(2)}_{\mathrm{E}00}\right] \\ &= 1 + \frac{1}{\left(h^{(1)}_{\mathrm{E}00} + \frac{F_1}{F_0}\phi_1\right)^2}\left[\left(\frac{F_1^2}{F_0^2} - \frac{2F_2}{F_0}\right)\phi_1^2 - \left(h^{(1)}_{\mathrm{E}00}\right)^2 - \frac{2F_1}{F_0}\phi_2 - 2h^{(2)}_{\mathrm{E}00}\right].\end{aligned} \tag{38}$$

Inserting the scalar field and metric components determined above, we obtain the PPN parameters for a

scalar-tensor theory formulated in the Einstein frame:

$$G_{\rm J}(r) = \frac{G}{F_0}\left(1 + \frac{F_1^2}{4F_0^2}e^{-m_{\rm E}r}\right) \tag{39a}$$

$$\gamma(r) = \frac{1 - \frac{F_1^2}{4F_0^2}e^{-m_{\rm E}r}}{1 + \frac{F_1^2}{4F_0^2}e^{-m_{\rm E}r}}. \tag{39b}$$

$$\begin{aligned}\beta(r) = 1 &+ \frac{F_1^2}{4F_0^2\left(1 + \frac{F_1^2}{4F_0^2}e^{-m_{\rm E}r}\right)^2}\left(\frac{F_1^2}{4F_0^2} - \frac{F_2}{2F_0}\right)e^{-2m_{\rm E}r} \\ &+ \frac{F_1^2 m_{\rm E} r}{32F_0^2\left(1 + \frac{F_1^2}{4F_0^2}e^{-m_{\rm E}r}\right)^2}\Big[8e^{-m_{\rm E}r}\ln m_{\rm E}r - 4e^{-2m_{\rm E}r} - 8\left(e^{m_{\rm E}r} + m_{\rm E}r\right)\mathrm{Ei}(-2m_{\rm E}r) \\ &\qquad + 3\frac{F_1}{F_0}\frac{V_3}{V_2}\left(e^{-m_{\rm E}r}\mathrm{Ei}(-m_{\rm E}r) - e^{m_{\rm E}r}\mathrm{Ei}(-3m_{\rm E}r)\right)\Big]\end{aligned} \tag{39c}$$

To compare this result to the one found in [10], we use the transformation laws for the coupling functions (A7) and the potentials (A8). Indeed, this leads to equations (9).

If we choose to neglect the second order deviation from the Schwarzschild metric (i.e. $h^{(2)}_{\rm E00} = -4G^2M_{\rm E}^2/(2r^2)$) and only consider the leading order scalar field contribution (i.e. we set $\phi_2 = 0$), then the effective coupling constant and the PPN parameters simplify to

$$G_{\rm J}(r) = \frac{G}{F_0}\left(1 + \frac{F_1}{2F_0}\frac{r}{GM_{\rm E}}\phi_1\right) \tag{40a}$$

$$\gamma(r) = \frac{1 - \frac{F_1}{2F_0}\frac{r}{GM_{\rm E}}\phi_1}{1 + \frac{F_1}{2F_0}\frac{r}{GM_{\rm E}}\phi_1} \tag{40b}$$

$$\beta(r) = 1 + \frac{\left(\frac{F_1^2}{4F_0^2} - \frac{F_2}{2F_0}\right)\phi_1^2}{\left(\frac{GM_{\rm E}}{r} + \frac{F_1}{2F_0}\phi_1\right)^2}. \tag{40c}$$

We notice that on the one hand, any non-trivial scalar-tensor theory predicts a γ different from its general relativity value 1. On the other hand, it is still possible to have $\beta = 1$: if $F_1^2/F_0 - 2F_2 = 0$. This condition is equivalent to $F'(\phi_0)^2/F(\phi_0) - F''(\phi_0) = 0$ which is solved by $F(\phi) = c_1\exp(c_2\phi)$. An exponential coupling function in the Einstein frame corresponds to a constant coupling function in the Jordan frame, $\omega = \omega_0$, and therefore to a Brans-Dicke-like theory as for instance the original chameleon model (see sections III A and III D).

In the following section we discuss current constraints on the PPN parameters and apply them to our formalism. In particular the constraint on γ coming from the Cassini spacecraft is discussed. This is followed by some important examples of scalar-tensor theories.

III. EXPERIMENTAL FRAMEWORK AND CONSTRAINTS

Above we have discussed the scalar field in vacuum outside a point source in the weak field limit. The assumption of a point source is obviously not correct for experiments performed around extended objects as the Earth or the Sun. Within such an object the field can behave very different to that of a point source and screening mechanisms can show up due to non-linear effects. But still, since the density in the solar system is very low, one can expect the field to maintain the form $\phi_1 \sim e^{-mr}/r$ in the low density region outside some source. Therefore, we make the ansatz

$$\varphi(\chi) = \varphi_0 + \varphi_1(\chi) = \varphi_0 + \xi\frac{2}{2\omega_0 + 3}\frac{GM_{\rm J}}{\chi}e^{-m_{\rm J}(\chi - X)} \tag{41a}$$

$$\phi(r) = \phi_0 + \phi_1(r) = \phi_0 + \xi\frac{F_1}{2F_0}\frac{GM_{\rm E}}{r}e^{-m_{\rm E}(r-R)} \tag{41b}$$

for the exterior field up to first order, written in the Jordan and the Einstein frame, respectively. By X (Jordan frame) and $R = \sqrt{F_0}X$ (Einstein frame) we denote the size of the object. Therefore, the field starts falling off exponentially at the surface of the source instead of at its center. Notice that we introduced some arbitrary parameter ξ. By doing so, we are able to discuss constraints on the PPN parameters around more realistic sources, also for theories containing screening mechanisms without knowing their exact nature. The ξ parameter describes how much the exterior field deviates from that generated by a point source ($\xi = 1$) with the same mass. In other words, a source can act as an effective point source of mass ξM. In particular, we will show in section III C that a massive Brans-Dicke scalar field takes this form if we consider the source to be a sphere with con-

stant density. We find an expression for ξ which depends on both the mass of the scalar field and the radius of the source.

Plugging the ansatz above into (40) we find the effective gravitational constant and the PPN parameters

$$\begin{aligned} G_{\mathrm{J}} &= \frac{G}{F_0}\left(1+\xi\frac{F_1^2}{4F_0^2}e^{-m_{\mathrm{E}}(r-R)}\right) \\ &= \frac{G}{\varphi_0}\left(1+\xi\frac{1}{2\omega_0+3}e^{-m_{\mathrm{J}}(\chi-X)}\right) \end{aligned} \tag{42a}$$

$$\gamma = \frac{1-\xi\frac{F_1^2}{4F_0^2}e^{-m_{\mathrm{E}}(r-R)}}{1+\xi\frac{F_1^2}{4F_0^2}e^{-m_{\mathrm{E}}(r-R)}} = \frac{1-\frac{\xi}{2\omega_0+3}e^{-m_{\mathrm{J}}(\chi-X)}}{1+\frac{\xi}{2\omega_0+3}e^{-m_{\mathrm{J}}(\chi-X)}} \tag{42b}$$

$$\begin{aligned} \beta &= 1+\frac{\left(1-\frac{2F_0F_2}{F_1^2}\right)}{\left[1+\left(\xi\frac{F_1^2}{4F_0^2}e^{-m_{\mathrm{E}}(r-R)}\right)^{-1}\right]^2} \\ &= 1+\frac{\frac{\varphi_0\omega_1}{2\omega_0+3}}{\left[1+\left(\xi\frac{1}{2\omega_0+3}e^{-m_{\mathrm{J}}(\chi-X)}\right)^{-1}\right]^2}. \end{aligned} \tag{42c}$$

Typically, experimental constraints on PPN parameters are used to limit the $(\omega_0, \tilde{m}_{\mathrm{J}})$-parameter space [7, 10]. The definition of the ω_0-independent mass

$$\tilde{m}_{\mathrm{J}} := \sqrt{2U_2\varphi_0} \tag{43}$$

is required in order to have two independent parameters since the original mass m_{J}, defined in (10), depends on ω_0. But since we want to incorporate possible screening mechanisms in extended sources, giving us the additional parameter ξ, we consider a slightly different approach. We define a new parameter

$$\alpha := \frac{\xi}{2\omega_0+3} = \xi\frac{F_1^2}{4F_0^2}, \tag{44}$$

allowing us to constrain the (α, m_{J})-parameter space. Notice that α contains two different kinds of parameters. First, the components of the scalar coupling functions, ω_0 and F_1^2/F_0^2, depend on the underlying theory of gravity only and are the same everywhere. Second, the parameter ξ can depend on properties of the source, as its composition. Therefore, it can vary drastically among different sources.

There are different experimental constraints on the PPN parameters. The most stringent one comes from measuring the frequency shift of a radio signal sent from and to the Cassini spacecraft while close to conjunction with the Sun, with $\gamma = 1 + (2.1 \pm 2.3)\cdot 10^{-5}$ at the 1σ-confidence level [14]. The closest distance between the propagating signal and the center of the Sun was 1.6 solar radii. We can now use this to constrain the parameter space $(\alpha_{\mathrm{Sun}}, m_{\mathrm{E}})$, as shown in figure 1.

The perihelion precession of Mercury gives the constraint $|2\gamma - \beta - 1| < 3\cdot 10^{-3}$ [6]. Planetary ephemerides are used to constrain $|\gamma - 1|$ and $|\beta - 1|$ to the 10^{-5}-level [18, 19]. But since the gravitational interaction does not take place at a fixed distance from some massive body, this limit cannot be used to constrain the distance dependent parameters discussed here.

Scalar theories can also be constrained by accurate measurements of the periods of binary pulsars: if scalar radiation is emitted, it results in a change of the orbital period [20].

The GAIA mission launched in 2013, located at the Sun-Earth Lagrange point L2, is expected to improve the constraint on γ to the 10^{-6} level [21] via relativistic astrometry by precisely monitoring the 3D motion of planets and stars in our galaxy.

In the following subsections, we consider specific theories of gravity and use the above formalism to calculate their PPN parameters. The Cassini measurement can then be used to constrain these theories. As atomic clocks become more accurate, clock carrying satellites that orbit the Earth will place constraints on the value of the PPN parameters around our own planet. We will discuss such measurements in Sec. IV.

A. Brans-Dicke theory

The simplest example and the prototype of scalar-tensor theories is Brans-Dicke theory [22]. In the Jordan frame it is defined to have a constant coupling $\omega = \omega_0$ and a vanishing scalar potential, leaving the field massless, $m_{\mathrm{J}} = 0$. Therefore, the PPN parameters will not have a distance dependence and we have $\xi = 1$ because no hiding mechanism occurs.

In this theory, ω_0 is the only parameter. With (A4) and (A5a) we obtain the coupling function $F(\phi) = F_0\exp[\pm 2(\phi-\phi_0)/\sqrt{2\omega_0+3}]$. Therefore, in the Einstein frame, Brans-Dicke theories have an exponential coupling function with no scalar potential term. This gives $\beta = 1$ as in general relativity and $\gamma = (\omega_0+1)/(\omega_0+2)$. Using the Cassini constraint on γ, one finds that $\omega_0 > 40'000$ at the 2σ-level.

B. Eddington-Robertson metric

Assuming that the potential vanishes $U = V = 0$ and then solving the equations of motion yields the PPN pa-

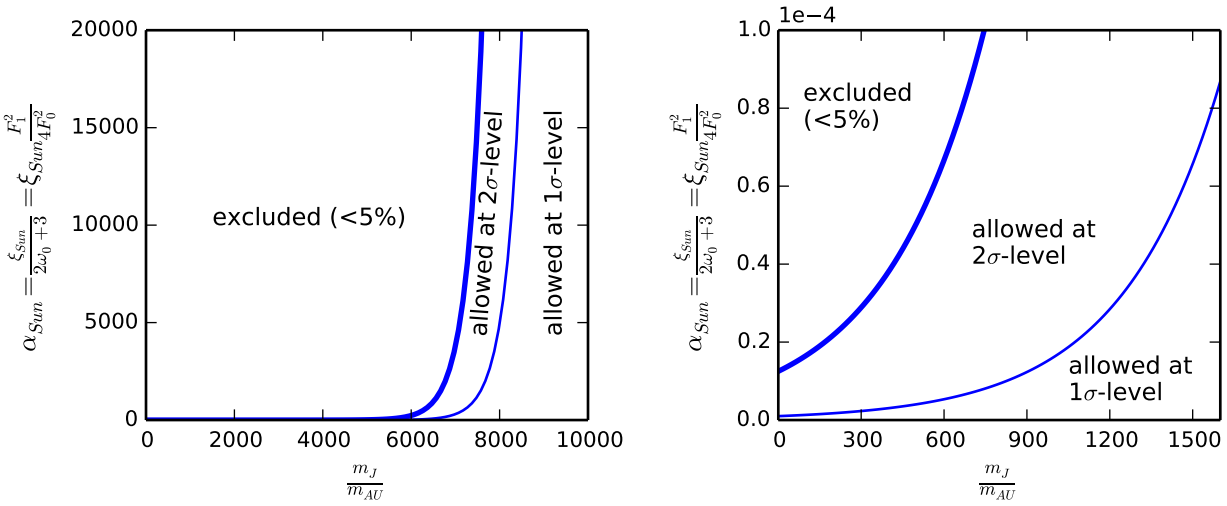

FIG. 1: Cassini constraint on scalar-tensor theories. The Cassini constraint $\gamma = 1 + (2.1 \pm 2.3) \cdot 10^{-5}$ (at 1σ-level) together with equation (42b) and $\chi - X_{\rm Sun} = 0.6$ solar radii $= 0.00279$AU are used to constrain the $(\alpha_{\rm Sun}, m_{\rm J})$-parameter space. The solid lines divide the plots into regions that are excluded (probability $< 5\%$) and that are allowed at the 2σ-level and at the $1\sigma-$level, respectively. The x-axis shows the mass, i.e. the inverse range, of the scalar field in the Jordan frame in terms of inverse astronomical units $m_{\rm AU} = 1/{\rm AU}$, the y-axis shows $\alpha_{\rm Sun} = \xi_{\rm Sun}/(2\omega_0 + 3) = \xi_{\rm Sun} F_1^2/(4F_0^2)$ where $\xi_{\rm Sun}$ is a parameter characteristic for the Sun.

rameters

$$G_{\rm J} = \frac{G}{\varphi_0}\left(1 + \frac{1}{2\omega_0 + 3}\right) = \frac{G}{F_0}\left(1 + \frac{F_1^2}{4F_0^2}\right) \tag{45a}$$

$$\gamma = \frac{1+\omega_0}{2+\omega_0} = \frac{1 - \frac{F_1^2}{4F_0^2}}{1 + \frac{F_1^2}{4F_0^2}} \tag{45b}$$

$$\beta = 1 + \frac{\varphi_0 \omega_1}{(2\omega_0+3)(2\omega_0+4)^2} = 1 + \frac{\frac{F_1^2}{4F_0^2}\left(\frac{F_1^2}{4F_0^2} - \frac{F_2}{2F_0}\right)}{\left(1 + \frac{F_1^2}{4F_0^2}\right)^2}. \tag{45c}$$

Due to the absence of the potential there is no distance dependence in both $G_{\rm J}$ and the PPN parameters. The metric (2) with these constant parameters was given by Eddington and Robertson [23]. So, for fixed values of γ and β we can invert this expressions to obtain the components of the coupling function in the Jordan frame

$$\omega_0 = -\frac{2\gamma - 1}{\gamma - 1} \tag{46a}$$

$$\omega_1 = -\frac{4(\beta - 1)(\gamma + 1)}{\varphi_0 (\gamma - 1)^3} \tag{46b}$$

and accordingly in the Einstein frame

$$\frac{F_1^2}{4F_0^2} = \frac{1-\gamma}{1+\gamma} \tag{47a}$$

$$\frac{F_2}{2F_0} = \frac{5 - 4\beta - 2\gamma + \gamma^2}{1 - \gamma^2}. \tag{47b}$$

C. Massive Brans-Dicke Theory

Here we solve the scalar field equation of a massive Brans-Dicke scalar field generated by a more realistic source than a point mass. We consider a coupling function which is, as in the original Brans-Dicke theory, exponential in the Einstein frame and thus constant ($\omega = \omega_0$) in the Jordan frame. Further, in the Einstein frame we add a quadratic potential $V = V_2(\phi - \phi_0)^2$ with $V_2 = 2m_{\rm E}$. This corresponds to the potential $U = U_2(\varphi - \varphi_0)^2$ in the Jordan frame.

For the case of a point source, constraints on massive Brans-Dicke fields have been discussed in [7, 10]. There, the authors used the Cassini constraint on γ to limit the $(\tilde{m}_{\rm J}, \omega_0)$-parameter space. Here, we extend this discussion by replacing the point source with a more realistic density distribution. This will allow us to determine the parameter ξ, introduced in (41).

We consider a static spherically symmetric mass with radius R and constant density ρ_{E0} (i.e. $\rho_E(r) = \rho_{E0}$ for $r < R$ and $\rho_E(r) = 0$ otherwise) and we neglect the gravitational effects of pressure. Further we assume that the mass is surrounded by vacuum. The equation of motion is given by

$$\left(\nabla_r^2 - m_{\rm E}^2\right)\phi_1(r) = -\frac{F_1}{F_0} 2\pi G \rho_{\rm E}(r), \tag{48}$$

which follows from (20). To solve this equation we make use of the Green function $G(\vec{r}) = -e^{-m_{\rm E} r}/4\pi r$, solving the equation $\left(\nabla_r^2 - m_{\rm E}^2\right) G(\vec{r}) = \delta(\vec{r})$. Then we find the

scalar field by integrating

$$\begin{aligned}\phi_1(\vec{r}) &= \int G(|(\vec{r})-(\vec{s})|)\left(-\frac{F_1}{F_0}2\pi G\rho_{\rm E}(s)\right)d^3\vec{s}\\ &= \frac{F_1}{F_0}\pi G\rho_{E0}\\ &\quad\times\int_0^\pi\int_0^R \frac{e^{-m_{\rm E}\sqrt{r^2+s^2-2rs\cos\theta}}}{\sqrt{r^2+s^2-2rs\cos\theta}}s^2\sin\theta\,ds\,d\theta.\end{aligned} \tag{49}$$

To obtain the exterior solution $\phi_1^{\rm ext}(r>R)$, the integrand is expanded around $s/r=0$, since $r>s$ for all s. This allows each term of the Taylor series to be integrated, giving

$$\begin{aligned}\phi_1^{\rm ext}(r>R) =&\frac{F_1}{F_0}\frac{\pi G\rho_{E0}}{r}e^{-m_{\rm E}r}\\ &\times\sum_{k=0}^{\infty}m_{\rm E}^{2k}R^{2k+3}\frac{2}{(2k+1)!(2k+3)}.\end{aligned} \tag{50}$$

Finally, this can be written as

$$\begin{aligned}\phi_1^{\rm ext}(r>R) =&\left(3\frac{m_{\rm E}R\cosh(m_{\rm E}R)-\sinh(m_{\rm E}R)}{R^3m_{\rm E}^3}e^{-m_{\rm E}R}\right)\\ &\times\frac{F_1}{2F_0}\frac{GM_{\rm E}}{r}e^{-m_{\rm E}(r-R)},\end{aligned} \tag{51}$$

where in the last step we substituted $M_{\rm E}=4\pi/3\rho_{E0}R^3$.

The interior solution $\phi_1^{\rm ext}(r<R)$ is obtained by splitting the integral over s into two parts. First, we perform the integral $\int_0^r$ where we can expand around $s/r=0$ and find the solution analogous to the exterior solution. Second, for the integral from $\int_r^R$ we can expand around $r/s=0$. Together, we find

$$\begin{aligned}\phi_1^{\rm int}(r<R) =&3\frac{F_1}{2F_0}\frac{GM_{\rm E}}{R^3}\left[\frac{e^{-m_{\rm E}r}}{m_{\rm E}^2}\left(\cosh(m_{\rm E}r)+\sinh(m_{\rm E}r)\right)\right.\\ &\left.-e^{-m_{\rm E}R}\frac{1+m_{\rm E}R}{m_{\rm E}^3r}\sinh(m_{\rm E}r)\right].\end{aligned} \tag{52}$$

Notice that the exterior solution (51) precisely coincides with the general ansatz (41) if we choose

$$\xi = 3\frac{m_{\rm E}R\cosh(m_{\rm E}R)-\sinh(m_{\rm E}R)}{R^3m_{\rm E}^3}e^{-m_{\rm E}R}. \tag{53}$$

The solution expressed in the Jordan frame is

$$\begin{aligned}\varphi_1^{\rm ext}(\chi>X) =&\left(3\frac{m_{\rm J}X\cosh(m_{\rm J}X)-\sinh(m_{\rm J}X)}{X^3m_{\rm J}^3}e^{-m_{\rm J}X}\right)\\ &\times\frac{2}{2\omega_0+3}\frac{GM_{\rm J}}{\chi}e^{-m_{\rm J}(\chi-X)}\\ \varphi_1^{\rm int}(\chi<X) =&\frac{6}{2\omega_0+3}\frac{GM_{\rm J}}{X^3}\\ &\times\left[\frac{e^{-m_{\rm J}\chi}}{m_{\rm J}^2}\left(\cosh(m_{\rm J}\chi)+\sinh(m_{\rm J}\chi)\right)\right.\\ &\left.-e^{-m_{\rm J}X}\frac{1+m_{\rm J}X}{m_{\rm J}^3\chi}\sinh(m_{\rm J}\chi)\right].\end{aligned} \tag{54}$$

Since the γ parameter (42b) depends on ξ, it depends on the size of the source. In the massless limit $m_{\rm E/J}\to 0$, ξ approaches unity. Then, γ depends on properties of the theory only and is independent of R. In the limit of vanishing radius, ξ approaches unity as well, giving the same result as for a point source.

While in [7] the interaction distance is assumed to be $r=1\,$AU, Hohmann *et al.* [10] choose $r=1.6$ solar radii since this is the closest distance between the signal and the Sun. This dramatically improves the constraints on $\tilde{m}_{\rm J}$ and ω_0. Including ξ given by (53), which accounts for the assumption that the Sun is a sphere with constant density, the constraint on the $(\tilde{m}_{\rm J},\omega_0)$-parameter space given by the Cassini experiment is shown in figure 2 (solid lines), where we assume that $r=1.6$ solar radii. Comparing to the dashed lines which represent the analogous result for a point source, we notice that the constraints are more stringent if an extended source is considered. This is due to the fact that, even though $\xi<1$, the field falls off like $e^{-m_{\rm E}(r-R)}$ instead of $e^{-m_{\rm E}r}$.

D. Chameleon theory

Another example of a class of scalar-tensor theories are chameleon theories, introduced by Khoury and Weltman [12]. They allow a very light cosmological scalar field that couples to matter with gravitational strength and satisfies current observational constraints. Formulated in the Einstein frame, chameleons have, as Brans-Dicke theory does, an exponential coupling function $F(\phi)=\exp(-2\sqrt{2}k_i\phi)$. The coupling constants k_i may vary for different matter species i, but for simplicity we assume that it takes the same value k for all kinds of matter. This assumption is taken in accordance to general relativity where gravitation couples universally to all matter species and thereby ensures that the weak equivalence principle is satisfied. The presence of a scalar field would lead to an additional (or *fifth*) force and consequently, a matter-dependent scalar coupling would lead to violations of the weak equivalence principles. A possible model to explain such a matter-dependent scalar coupling is given by Damour and Donoghue [24].

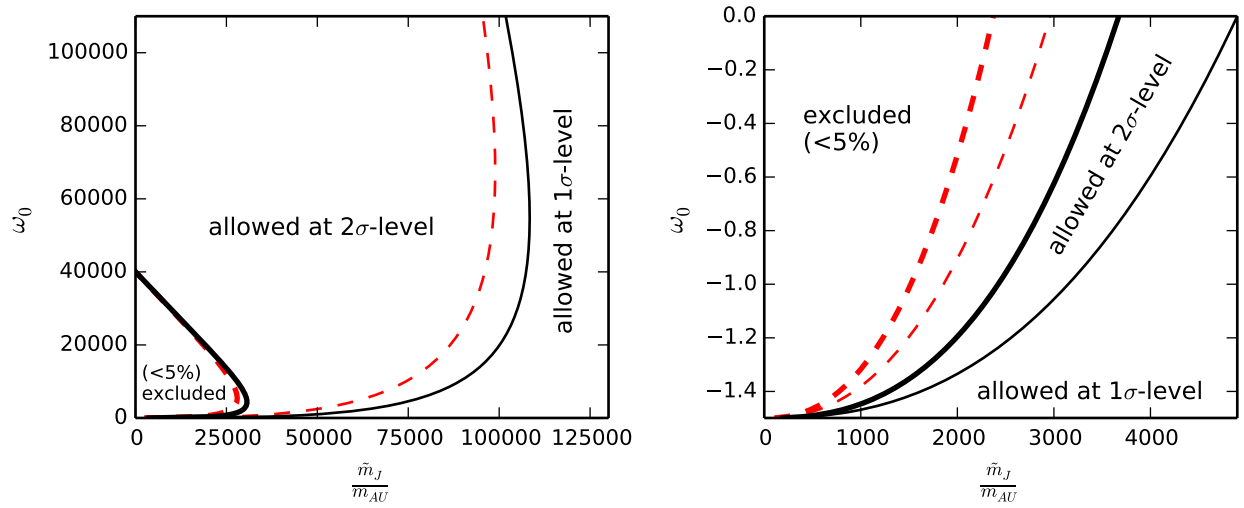

FIG. 2: Cassini constraint on massive Brans-Dicke theory. The constraint on PPN γ given by the Cassini experiment is used to constrain the $(\tilde{m}_J, \omega_0)$-parameter space for massive Brans-Dicke theory. For this theory, the parameter ξ in the expression for γ is given by (53). For the interaction distance we take $\chi - X_{\rm Sun} = 0.6$ solar radii. The solid lines separate the regions which are excluded (probability $< 5\%$), that are allowed at the $2\sigma-$level and at the $1\sigma-$level, respectively. The dashed-lines show the corresponding boundaries between these regions for the case where the Sun is considered to be a point mass. The x-axis shows the ω_0-independent mass $\tilde{m}_{\rm J}$ in terms of inverse astronomical units $m_{\rm AU} = 1/{\rm AU}$, the y-axis shows ω_0.

In contrast to Brans-Dicke, chameleons have a scalar potential, giving the field a mass and therefore a finite range. Typically, runaway potentials like an inverse power-law potential $V \sim \phi^{-n}$ are considered. The interplay between such a potential and the exponential coupling causes the range of the scalar field to depend on the surrounding matter density. In a dense region, like inside the Earth or within its atmosphere, the scalar field becomes so massive that the force corresponding to the scalar field becomes short ranged. This hiding feature makes it very difficult to detect the chameleon field with Earth-based experiments. On larger scales the field is long ranged and it might be detectable by experiments performed in space.

The exterior scalar field generated by a compact object like a planet or a star is determined only by the very outer layer of the object, we say that it has a thin shell. It is shown in [12] that the exterior field is

$$\phi(r) = \phi_0 - 3\delta\sqrt{2}k\frac{GM_{\rm E}}{r}e^{-m_{\rm E}(r-R)}, \qquad (55)$$

where $\delta := \Delta R/R \ll 1$ is the thin shell parameter. The chameleon field profile corresponds to the field (41) with $\xi = 3\delta$, giving the parameter

$$\gamma(r) = \frac{1 - 6\delta k^2 e^{-m_{\rm E}(r-R)}}{1 + 6\delta k^2 e^{-m_{\rm E}(r-R)}}. \qquad (56)$$

This is the same result as found in [8]. Furthermore, $\beta = 1$ holds since the coupling is mediated by an exponential function.

The thin shell factor is proportional to $(\phi_\infty - \phi_c)/k\Phi_c$ where $\Phi_c = GM/R$ is the Newtonian potential of an object at its surface or, in other words, its compactness. ϕ_c and ϕ_∞ are the field values inside and infinitely far away from the compact object. They are density dependent and therefore the thin shell parameter depends on the composition of an object. Typically it holds that $\phi_\infty \gg \phi_c$, such that approximately $\delta \sim \phi_\infty/k\Phi_c$, allowing us to compare the ability of testing chameleons around different compact objects in the solar system just by comparing their Newtonian potentials Φ_c. From this point of view, the Sun is not a promising candidate to probe chameleons due to its high compactness. The Earth, and even better the Moon, are more appropriate.

The Cassini experiment can be used to constrain the $(\delta_{\rm Sun}, m_{\rm E})$-parameter space for fixed k using equation (56). For $k \sim 1$ and small masses for the scalar field, this constraints $\delta_{\rm Sun}$ to the 10^{-6} level. For larger masses the thin-shell factor may take much larger values. A constraint of γ in Earth orbit would produce the analogous result but for the thin-shell factor of the Earth.

It is important to keep in mind that also a satellite which aims to probe gravity is not a test mass and can therefore acquire a thin shell itself. This would further suppress any GR-violating signals. Khoury and Weltman estimate that a typical satellite does not have a thin shell if the condition $10^{-15} < \delta < 10^{-7}$ is satisfied [12].

In [8] it is argued that chameleons are ruled out due to the incompatibility of solar system and cosmological

constraints. But anyway, they provide an interesting example of a theory predicting deviations from general relativity which depend not only on the distance from some massive object but also on its mass, radius and composition. It is not only important to probe gravity to high levels of accuracy, but also around different celestial bodies.

IV. MEASURING PPN PARAMETERS IN EARTH'S EXTERIOR FIELD

In 2016, the Atomic Clock Ensemble in Space (ACES) mission will place an atomic clock on the International Space Station (ISS) that is expected to reach a fractional frequency uncertainty of $\Delta f/f \sim 10^{-16}$ [15]. In the future, space clocks will continue to improve. After ACES, there are plans to put an optical clock on the ISS as part of the Space Optical Clock (SOC) project. The best optical clocks on Earth have already reached accuracies of $\Delta f/f \sim 10^{-18}$ over an integration period of 25000 sec [25, 26], and significant progress is being made towards building optical clocks that are mobile, more compact and more reliable.

In this section we investigate the effect that the PPN parameters have on a satellite that carries an atomic clock and orbits the Earth. In this experiment, a precise clock on a satellite broadcasts tick signals down to a terrestrial receiving station which records their arrival times using a local, more accurate clock. The rate at which the ticks arrive is the redshift. This setup allows the orbit to be tracked down to the clock accuracy. For given Keplerian initial conditions, we simulate both the general relativistic orbit as well as the orbit in an alternative theory of gravity with parameters different from those of general relativity. This solves the forward problem, and taking the difference of these two signals provides a way to give upper limits on how well the PPN parameters can be constrained by this type of mission. To investigate PPN parameter predictability more thoroughly, the full inverse problem needs to be solved, which entails reconstructing the full four-dimensional trajectory of the satellite by fitting different models to redshift data. Mock redshift data can be generated from solutions to the forward problem with different parameters and added noise. We leave attempts to solve the inverse problem to future work.

We choose an eccentric orbit like that originally proposed for STE-QUEST [16]. We solve the forward problem using the code introduced by Angélil *et al.* [11, 27]. Note that the effects that the PPN parameters have on the orbit dominate, while their effects on the light path between the emitter and the receiver are about two orders of magnitude smaller [11, 27].

The trajectory of a spacecraft in Earth's external field is found by integrating Hamilton's equations. We have seen that for general scalar-tensor theories the PPN parameters depend on the location where they are tested. If the potential is set to zero, making the field massless, the PPN parameters γ and β are constant (see section III B). The corresponding metric in the Jordan frame is

$$g_{tt} = -1 + \frac{2GM}{r}\epsilon - \frac{2G^2M^2}{r^2}(\beta-\gamma)\,\epsilon^2 \tag{57a}$$

$$g_{rr} = 1 + \frac{2GM}{r}\gamma\epsilon \tag{57b}$$

$$g_{\theta\theta} = r^2 \tag{57c}$$

$$g_{\varphi\varphi} = r^2\sin^2\theta, \tag{57d}$$

where we consider non-isotropic Schwarzschild coordinates. (We write r instead of χ for the radial coordinate and drop all J-indices.) This is a special case of (B4) with $A(r) = 1, B(r) = \beta$ and $C(r) = \gamma$. The corresponding Hamiltonian for a satellite's trajectory in Earth's external field is obtained from (C1)

$$\begin{aligned} H &= -\frac{p_t^2}{2} + \left[-\frac{GMp_t^2}{r} + \frac{p_r^2}{2} + \frac{p_\theta^2}{2r^2} + \frac{p_\varphi^2}{2r^2\sin^2\theta}\right]\epsilon + \left[-\frac{2G^2M^2p_t^2}{r^2}\left(1 - \frac{1}{2}\beta + \frac{1}{2}\gamma\right) - \frac{GMp_r^2}{r}\gamma\right]\epsilon^2 \\ &= -\frac{p_t^2}{2} + \left[-\frac{GMp_t^2}{r} + \frac{\vec{p}^2}{2}\right]\epsilon + \left[-\frac{2G^2M^2p_t^2}{r^2}\left(1 - \frac{1}{2}\beta + \frac{1}{2}\gamma\right) - \frac{GM}{r}\frac{(\vec{x}\cdot\vec{p})^2}{r^2}\gamma\right]\epsilon^2, \end{aligned} \tag{58}$$

where we change to Cartesian coordinates in the second line. Notice that β does not show up individually, but only in combination with γ. The equations of motion are given by Hamilton's equations.

We specify the orbit by choosing Keplerian initial conditions. We position the Earth-clock beneath perihelion, the satellite's point of closest approach. Hamilton's equations are integrated over 4.5 orbits, once for the general relativistic metric ($\gamma = \beta = 1$), giving the redshift signal z_{GR}, and then for one where these parameters slightly differ from unity, giving $z_{\text{non-GR}}$. Taking the difference of the two signals,

$$\Delta z = z_{\text{GR}} - z_{\text{non-GR}}, \tag{59}$$

allows us to find the maximum difference in the redshift, $|\Delta z|_{\max}$, averaged over one orbit. Such a difference in the redshift signal should be detectable if this residual redshift is within the accuracy of the experiment.

There are numerous both relativistic and non-relativistic effects which enter the dynamics that have not been considered here. They will need to be accurately modeled as part of the parameter recovery procedure. Non-relativistic effects include atmospheric drag, solar radiation pressure and Earth's Newtonian multipole field. Angélil *et al.* (2014) [11] calculate a host of general relativistic effects on the satellite and the light-path trajectories. The γ and β variations discussed in this paper correspond to modified Schwarzschild terms in the Hamiltonian. The standard GR frame-dragging effect, the Shapiro effect (bent light paths), spin-squared effects on the orbit, as well as further yet weaker effects would need to be included when searching for deviations from non-GR values of γ and β. Effects that come into play at different orders (refer to different blocks in table 1 in [11]) will not be degenerate with one another due to their fundamentally different $r-$dependence, provided the satellite trajectory is elliptical, inducing a sufficient field strength modulation over the course of the integration time. Further discussion on these effects may also be found in [28].

In our approach, where we subtract the redshift signal predicted by general relativity from that with different PPN parameters, all these effects will cancel out in the subtraction process. A further approximation made is to allow the Earth to be transparent to the tick signals. In reality, however, certain portions of the experiment would miss data during line-of-sight loss. This would be in part compensated by having multiple ground stations so that at any given point a clock on Earth will be within the satellite's line of sight.

We choose an eccentric orbit with semi-major axis $a = 32'090\,\mathrm{km}$ and eccentricity $e = 0.779$. Such an orbit has a perihelion distance of 7092 km, corresponding to an altitude of about 700 km above ground. This orbit was chosen for the original proposal of the satellite mission STE-QUEST [16] and we take it as our reference orbit. We then compare the general relativity orbit to the orbit with PPN parameters differing from unity by subtracting the redshift signal of the modified orbit from the general relativistic orbit. Figure 3 shows the result for the choice $\gamma = 1 + 10^{-5}$, $\beta = 1$.

We find that the difference peaks around pericenter, and builds up with every orbit. For just one orbit we can read off the maximum difference in redshift $\Delta z = 2 \cdot 10^{-15}$.

The absolute value of the maximum difference in the redshift signal over one orbit, indicated by its color/grey scale, is plotted for a range of parameters in figure 4. It is evident that, theoretically, using a clock of accuracy $\Delta f/f \sim 10^{-16}$ one should be able to constrain $|\gamma - 1| \sim |\beta - 1| \sim 10^{-6}$.

Along lines with $\beta - \gamma =$ constant the absolute value of the signal is the same. This comes from the fact that the signal is mainly caused by the term in the Hamiltonian (58) proportional to $\tilde{\beta} := 1 - (\beta - \gamma)/2$, while the effect of the one proportional to γ is negligible. Therefore, $|\tilde{\beta} - 1|$ remains the same if β and γ are interchanged, while the sign of the difference in the redshift signal flips.

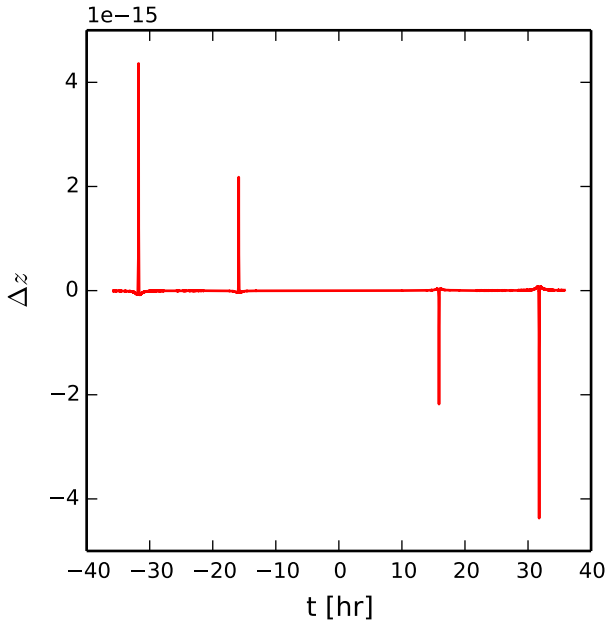

FIG. 3: Difference in Redshift Curve. The difference in the redshift signal between the GR-orbit and the orbit with $\gamma = 1 + 10^{-5}$ and $\beta = 1$, $\Delta z = z_{\mathrm{GR}} - z_{\text{non-GR}}$, is plotted as a function of time t (in hours).

Thus, having a clock on our reference orbit would allow to perform interesting tests of gravitational effects. It is instructive to examine several kinds of orbits to see which ones provide the strongest residuals. On the one hand, we want the satellite to pass by the Earth closely, therefore having a small pericenter distance in order to have strong gravitational effects. On the other hand, it should be far enough to minimize effects as inhomogeneities of the Earth's gravitational potential or atmospheric drag [28]. We fix the pericenter distance at $d = 700\,\mathrm{km}$ above the ground. Then, we vary the eccentricity from a circular orbit $e = 0$ to a highly eccentric orbit $e = 0.9$, or equivalently, we vary the semi-major axis a from the pericenter distance (circular orbit) up to $71'000\,\mathrm{km}$. These quantities are related by $d = a(1 - e)$. In figure 5, the maximum difference in the redshift signal over one orbit between general relativity and some scalar-tensor theories with different $\gamma \neq 1$ are shown as a function of the eccentricity and the semi-major axis. We notice that for increasing eccentricity the magnitude of the signal increases significantly.

Now, we investigate the widths of the peaks of the difference in the redshift signals. The peaks are approximated by fitting a Lorentzian $f(t) = A/(2\pi)\Gamma[(t - t_0)^2 + \Gamma^2/4]^{-1} + d$, an example is shown in figure 6. From the fit we can easily determine the full width at half maximum. In figure 5, the peak width is plotted against the eccentricity for the case $\gamma = 1 + 10^{-5}$ and $\beta = 1$. Even though

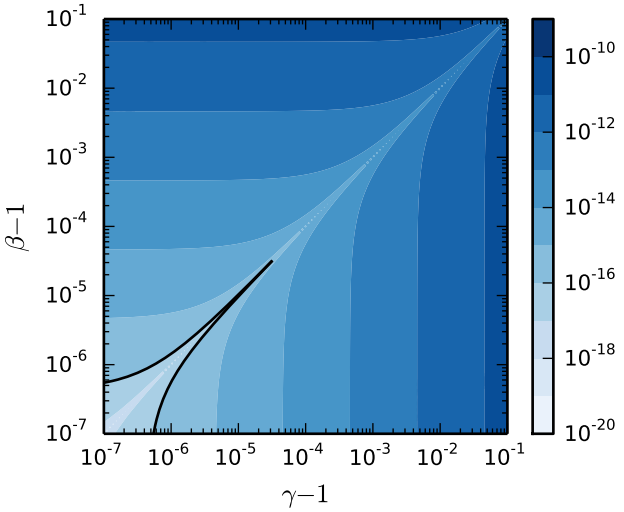

FIG. 4: Logarithmic parameter space plot. This parameter space plot shows the maximum difference in the redshift between the GR-orbit and that for a range of positive values for γ and β over one orbit. The solid line corresponds to the value 10^{-16}. For the orbit we chose our reference orbit.

the width decreases for growing eccentricities, its value is remains of order ~ 100 seconds: this is the time scale that needs to be resolved in order to find deviations coming from non-unity PPN parameters. While the width depends on the orbit, it is essentially independent of the PPN parameters, as the values change very little in the investigated range.

V. CONCLUSION

We calculate the PPN parameters γ and β for scalar-tensor theories formulated in the Einstein frame for the case of a point-like source. This extends the discussion of such theories in the Jordan frame given in [10]. To discuss tests of gravitation in the vicinity of more realistic sources we introduce a simple formalism which can take into account effects arising from the finite size of the source. We use the Cassini limit on PPN γ to put constraints on this formalism. In particular, we update the constraints on the parameter space of massive Brans-Dicke scalar fields by replacing the assumption of a point source with that of a constant-density sphere. This provides more stringent constraints since the proximity to the source is increased due to the extended radius of the object.

We emphasize that the presence of a scalar potential makes the field finitely ranged and therefore it is crucial to perform tests of gravitation at different distances. Additionally, performing experiments around different sources is particularly interesting because the exterior field profile is likely to depend on properties of an object like its compactness or its composition.

In the second part of the paper we discuss the possibility of testing scalar-tensor theories in Earth orbit using atomic clocks. Their rapid development and the current interest in satellite missions carrying such clocks opens the possibility to perform comprehensive tests of gravitation within the next decade. Such missions will provide constraints on the PPN parameters in the vicinity of the Earth. We calculate the relativistic effects on the satellite orbit coming from non-GR parameters γ and β. High-performance atomic clocks are sensitive to the associated change in the redshift signal. We find that with currently available clock technology and reasonable choices of spacecraft orbits one should be able to constrain $|\gamma-1| \sim |\beta-1| \sim 10^{-6}$. Our estimates provide upper limits to PPN parameters that could be measured by a clock in orbit. However, in order to provide more definite answers on possible constraints, one would have to solve the full inverse problem, where the relevant parameters are reconstructed from a redshift signal that contains all relevant effects. We show that a PPN parameter varying from one produces a change in the redshift signal, peaking around pericenter of the eccentric orbit. While the magnitude of the peak is determined by both the value of the parameters and the chosen orbit, its width, and therefore the time-scale which needs to be resolved, depends only on the orbit specifications.

ACKNOWLEDGMENTS

We acknowledge support from the Swiss National Science Foundation. R.B. also received support from the Dr. Tomalla Foundation. We thank the referee for constructive comments.

Appendix A: Conformal transformation between Jordan and Einstein frame

In this section, we discuss the conformal transformation relating the metrics in the Jordan and the Einstein frame. Starting in the Jordan frame (the converse is equivalent), we define the Einstein frame metric by $g^{\rm E}_{\mu\nu} := \varphi g^{\rm J}_{\mu\nu}$. For the square-root of the trace of the metric and the Ricci scalars it holds $\sqrt{-g_{\rm J}} = \varphi^{-2}\sqrt{-g_{\rm E}}$ and $R_{\rm J} = \varphi\left[R_{\rm E} + 6\nabla^2_{\rm E}\ln\varphi^{1/2} - 6(\nabla_{\rm E}\ln\varphi^{1/2})^2\right]$, respectively [29]. Plugging this into the Jordan frame action (4) and integrating by parts yields

$$S = \int d^4x\sqrt{-g_{\rm E}}\frac{M^2_{\rm Pl}}{2}\left[R_{\rm E} - \frac{2\omega+3}{2\varphi^2}\left(\nabla_{\rm E}\varphi\right)^2 - V\right] + \int d^4x\sqrt{-g_{\rm E}}\mathcal{L}^{\rm E}_{\rm m}(\Phi_{\rm m}, \varphi^{-1}g^{\rm E}_{\mu\nu}),$$

where we defined $V := \varphi^{-2}U$ and $\mathcal{L}^{\rm E}_{\rm m} := \varphi^{-2}\mathcal{L}^{\rm J}_{\rm m}$. To bring this into the desired form (6) we define a new scalar

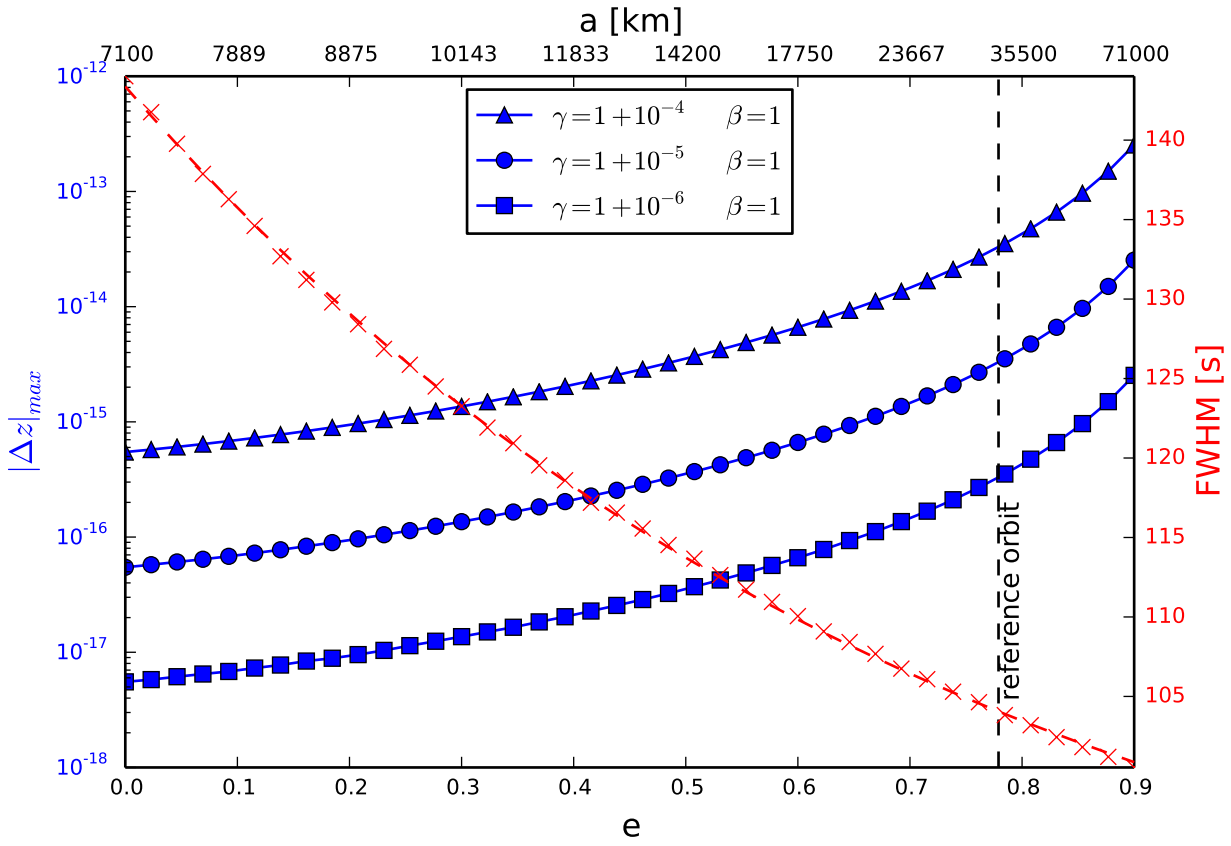

FIG. 5: Redshift signal and peak width as a function of eccentricity. We compare the GR-orbit to ones where γ slightly deviates from one. While the pericenter distance is fixed at $d = 7100\,\mathrm{km}$, i.e. about 700 km above ground, the eccentricity e, or equivalently the semi-major axis a, is changed. The triangle, circle and square data points show the maximum difference in the redshift signal, $|\Delta z|_{\max}$, for one orbit. The cross data points show the full width at half maximum (FWHM) for a signal peak for $\gamma = 1 + 10^{-5}$ and $\beta = 1$. The analogous for other choices of the parameters are omitted since they would yield the same result: the width is essentially constant for varying PPN parameters. We notice that the duration of the peak is of order 100 seconds for all eccentricities. This is the time scale which needs to be resolved to detect possible variations of the PPN parameters from their GR values.

field ϕ by demanding

$$-2(\nabla_{\mathrm{E}}\phi)^2 = -\frac{2\omega+3}{2\varphi^2}\left(\nabla_{\mathrm{E}}\varphi\right)^2, \tag{A1}$$

implying

$$\left(\frac{\partial\phi}{\partial\varphi}\right)^2 = \frac{2\omega+3}{4\varphi^2}. \tag{A2}$$

Defining the Einstein frame coupling function by $F := \varphi$, we obtain

$$\left(\frac{\partial F}{\partial\phi}\right)^2 = \frac{4F^2}{2\omega+3}. \tag{A3}$$

This requires $\omega > -3/2$ everywhere, and therefore $\omega_0 > -3/2$. Solving for ω yields

$$\omega = 2F^2\left(\frac{\partial F}{\partial\phi}\right)^{-2} - \frac{3}{2}. \tag{A4}$$

Using $F = \varphi$ and expanding both expressions in powers of ϵ

$$F = F_0 + F_1(\phi-\phi_0) + F_2(\phi-\phi_0)^2 \tag{A5a}$$
$$\varphi = \varphi_0 + \varphi_1\epsilon + \varphi_2\epsilon^2, \tag{A5b}$$

one obtains

$$\begin{aligned} &\varphi_0 = F_0 \qquad \varphi_1 = F_1\phi_1 \qquad \varphi_2 = F_2\phi_1^2 + F_1\phi_2 \\ &\phi_1 = \frac{1}{F_1}\varphi_1 \qquad \phi_2 = \frac{1}{F_1}\varphi_2 - \frac{F_2}{F_1^3}\varphi_1^2. \end{aligned} \tag{A6}$$

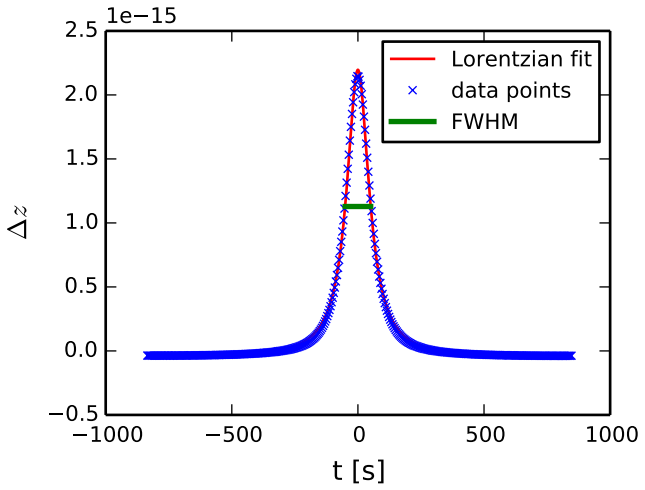

FIG. 6: Lorentzian fit of a peak. The data points show the difference in the redshift signal between a GR-orbit and $\gamma = 1 + 10^{-5}$, $\beta = 1$, as a function of time (in seconds), centered around pericenter. A Lorentzian $f(t) = A/(2\pi)\Gamma[(t-t_0)^2 + \Gamma^2/4]^{-1} + d$ is fitted, allowing to determine the full width at half maximum.

The relations between the coefficients of the couplings in the two frames are given by

$$\begin{aligned} \omega_0 &= \frac{2F_0^2}{F_1^2} - \frac{3}{2} \qquad \omega_1 = \frac{4F_0}{F_1^2} - \frac{8F_0^2F_2}{F_1^4} \\ F_0 &= \varphi_0 \qquad F_1 = \pm\frac{2\varphi_0}{\sqrt{2\omega_0+3}} \\ F_2 &= \frac{2\varphi_0}{2\omega_0+3}\left(1 - \frac{\varphi_0\omega_1}{2\omega_0+3}\right), \end{aligned} \tag{A7}$$

and for the potentials, using $U = F^2V$, one finds

$$\begin{aligned} U_2 &= \frac{F_0^2}{F_1^2}V_2 \qquad U_3 = \frac{2F_0}{F_1^2}\left(1 - \frac{F_0F_2}{F_1^2}\right)V_2 + \frac{F_0^2}{F_1^3}V_3 \\ V_2 &= \frac{4}{2\omega_0+3}U_2 \\ V_3 &= \pm\frac{8}{(2\omega_0+3)^{3/2}}\left[-\left(1 + \frac{\varphi_0\omega_1}{2\omega_0+3}\right)U_2 + \varphi_0 U_3\right]. \end{aligned} \tag{A8}$$

The coordinates in the two frames are related by $t_\mathrm{J} = t_\mathrm{E}/\sqrt{F_0}$ and $\chi = r/\sqrt{F_0}$. Note, there is a $\pm$-ambiguity when going from the Jordan to the Einstein frame: two theories in the Einstein frame related by $F_1, V_3 \leftrightarrow -F_1, -V_3$ correspond to the same theory in the Jordan frame.

Appendix B: Metric in non-isotropic coordinates

The PPN parameters are defined by introducing parameters to the individual terms of the expanded Schwarzschild metric written in isotropic coordinates. But often it is useful to consider the metric expressed in non-isotropic coordinates. This is achieved by defining a new radial coordinate r while the other coordinates remain the same. (Don't confuse the notion of r with the radial coordinate in the Einstein frame used earlier on.) We write the metric in isotropic coordinates in the general form

$$g_{tt} = -\left(1 - \frac{2GM}{\chi}A(\chi)\epsilon + \frac{2G^2M^2}{\chi^2}B(\chi)\epsilon^2\right) + \mathcal{O}(\epsilon^3) \tag{B1a}$$

$$g_{\chi\chi} = 1 + \frac{2GM}{\chi}C(\chi)\epsilon + \mathcal{O}(\epsilon^2) \tag{B1b}$$

$$g_{\theta\theta} = \left(1 + \frac{2GM}{\chi}C(\chi)\epsilon\right)\chi^2 + \mathcal{O}(\epsilon^2) \tag{B1c}$$

$$g_{\varphi\varphi} = \left(1 + \frac{2GM}{\chi}C(\chi)\epsilon\right)\chi^2\sin^2\theta + \mathcal{O}(\epsilon^2). \tag{B1d}$$

By introducing a new radial coordinate

$$r := \chi\left(1 + \frac{2GM}{4\chi}C(\chi)\epsilon\right)^2, \tag{B2}$$

which can be inverted to (outside the Schwarzschild radius)

$$\chi = r\left(\frac{1}{2} - \frac{GM}{2r}C(r)\epsilon + \frac{1}{2}\sqrt{1 - \frac{2GM}{r}C(r)\epsilon}\right), \tag{B3}$$

we obtain

$$g_{tt} = -1 + \frac{2GM}{r}A(r)\epsilon - \frac{2G^2M^2}{r^2}\left[B(r) - A(r)C(r)\right]\epsilon^2 \tag{B4a}$$

$$g_{rr} = 1 + \frac{2GM}{r}\left[C(r) - C'(r)r\right]\epsilon \tag{B4b}$$

$$g_{\theta\theta} = r^2 \tag{B4c}$$

$$g_{\varphi\varphi} = r^2\sin^2\theta. \tag{B4d}$$

Here, we used that $g_{\chi\chi}d\chi^2 = g_{rr}dr^2$. Transforming to Cartesian coordinates, the metric becomes

$$g_{tt} = -1 + \frac{2GM}{r}A(r)\epsilon - \frac{2G^2M^2}{r^2}\left[B(r) - A(r)C(r)\right]\epsilon^2 \tag{B5a}$$

$$g_{x_ix_j} = \delta_{ij} + \frac{2GM}{r}\left[C(r) - C'(r)r\right]\frac{x_ix_j}{r^2}\epsilon \tag{B5b}$$

where we used $F(r)dr^2 + r^2d\theta^2 + r^2\sin^2\theta d\varphi^2 = d\vec{x}^2 + \left[F(r) - 1\right](\vec{x}/r d\vec{x})^2$.

Appendix C: Hamiltonian

The Hamiltonian is given by $H = 1/2 g^{\mu\nu}p_\mu p_\nu$, where p_μ is the canonical four-momentum. Here, we consider the metric (B4), which we expand in powers of

$\epsilon \sim GM/r$. The orbital velocity of a non-relativistic particle in a weak gravitational field is $v \approx \sqrt{GM/r} \sim \epsilon^{1/2}$, requiring $p_r, p_\theta/r, p_\varphi/(r\sin\theta) \sim v \sim \epsilon^{1/2}$. Plugging the inverse metric into the formula for the Hamiltonian and assigning the terms to the appropriate orders in ϵ yields

$$\begin{aligned} H = &-\frac{p_t^2}{2} + \left[-\frac{GMp_t^2}{r}A(r) + \frac{p_r^2}{2} + \frac{p_\theta^2}{2r^2} + \frac{p_\varphi^2}{2r^2\sin^2\theta}\right]\epsilon \\ &+ \left[-\frac{2G^2M^2p_t^2}{r^2}\left(A(r)^2 - \frac{1}{2}B(r) + \frac{1}{2}A(r)C(r)\right)\right. \\ &\left. - \frac{GMp_r^2}{r}\left(C(r) - rC'(r)\right)\right]\epsilon^2. \end{aligned} \tag{C1}$$

From this it is evident why we drop all terms in the spatial metric components that are second and higher order in ϵ: they contribute to the Hamiltonian at third and higher orders. Notice that the expansion of the Hamiltonian for a signal propagating in the same spacetime looks different, since, even though we start with the same Hamiltonian, some terms contribute at different orders. This comes from the fact that photons travel with the speed of light and therefore, $p_t, p_r, p_\theta/r$ and $p_\varphi/(r\sin\theta)$ are of order 1. The equations of motion are given by Hamilton's equations $dp_\mu/d\lambda = -\partial H/\partial x^\mu$ and $dx^\mu/d\lambda = \partial H/\partial p_\mu$.

[1] Y. M. Cho and P. G. O. Freund, Phys. Rev. D **12**, 1711 (1975).
[2] T. Damour and A. M. Polyakov, Nuclear Physics B **423**, 532 (1994).
[3] G. Aad *et al.* (ATLAS Collaboration), Physics Letters B **726**, 120 (2013).
[4] A. H. Guth, Phys. Rev. D **23**, 347 (1981).
[5] S. M. Carroll, Phys. Rev. Lett. **81**, 3067 (1998).
[6] C. M. Will, Living Reviews in Relativity **17** (2014), 10.12942/lrr-2014-4.
[7] L. Perivolaropoulos, Phys. Rev. D **81**, 047501 (2010).
[8] A. Hees and A. Füzfa, Phys. Rev. D **85**, 103005 (2012).
[9] X.-M. Deng, Y. Xie, and T.-Y. Huang, Phys. Rev. D **79**, 044014 (2009).
[10] M. Hohmann, L. Järv, P. Kuusk, and E. Randla, Phys. Rev. D **88**, 084054 (2013).
[11] R. Angélil, P. Saha, R. Bondarescu, P. Jetzer, A. Schärer, and A. Lundgren, Phys. Rev. D **89**, 064067 (2014).
[12] J. Khoury and A. Weltman, Phys. Rev. Lett. **93**, 171104 (2004); Phys. Rev. D **69**, 044026 (2004).
[13] K. Hinterbichler and J. Khoury, Phys. Rev. Lett. **104**, 231301 (2010); K. Hinterbichler, J. Khoury, A. Levy, and A. Matas, Phys. Rev. D **84**, 103521 (2011).
[14] B. Bertotti, L. Iess, and P. Tortora, Nature **425**, 374 (2003).
[15] L. Cacciapuoti and C. Salomon, The European Physical Journal Special Topics **172**, 57 (2009).
[16] STE-QUEST team, ESA/SRE **6** (2013); B. Altschul *et al.*, arXiv.org: 1404.4307.
[17] C. M. Will, *Theory and Experiment in Gravitational Physics* (Cambridge University Press, 1993).
[18] A. K. Verma, A. Fienga, J. Laskar, H. Manche, and M. Gastineau, A & A **561**, A115 (2014).
[19] E. V. Pitjeva and N. P. Pitjev, Monthly Notices of the Royal Astronomical Society **432**, 3431 (2013).
[20] P. Brax, A.-C. Davis, and J. Sakstein, arXiv.org: 1301.5587.
[21] D. Hobbs, B. Holl, L. Lindegren, F. Raison, S. Klioner, and A. Butkevich, in *Relativity in Fundamental Astronomy: Dynamics, Reference Frames, and Data Analysis*, Proceedings of the International Astronomical Union, Vol. 5 (2009) pp. 315–319.
[22] C. Brans and R. H. Dicke, Phys. Rev. **124**, 925 (1961).
[23] S. Weinberg, *Gravitation and Cosmology: Principles and Applications of the General Theory of Relativity* (John Wiley & Sons, Inc., 1972).
[24] T. Damour and J. F. Donoghue, Phys. Rev. D **82**, 084033 (2010).
[25] N. Poli, C. W. Oates, P. Gill, and G. M. Tino, arXiv.org: 1401.2378.
[26] B. J. Bloom, T. L. Nicholson, J. R. Williams, S. L. Campbell, M. Bishof, X. Zhang, W. Zhang, S. L. Bromley, and J. Ye, Nature **506**, 71 (2014).
[27] R. Angélil and P. Saha, The Astrophysical Journal **711**, 157 (2010).
[28] J. Páramos and G. Hechenblaikner, Planetary and Space Science **79–80**, 76 (2013).
[29] Y. Fujii and K.-I. Maeda, *The Scalar-Tensor Theory of Gravitation* (Cambridge University Press, Cambridge, 2003).